Nonlinear Vibration of Gears With Tooth Surface Modifications

Tugan Eritenel
Mem. ASME
Department of Mechanical Engineering,
The Ohio State University,
Columbus, OH 43210
e-mail: eritenel.1@osu.edu

Robert G. Parker[1]
Research Professor
Fellow ASME
The Ohio State University,
Columbus, OH 43210;
Distinguished Professor Chair and
Executive Dean,
University of Michigan–Shanghai
Jiao Tong University Joint Institute,
Shanghai Jiao Tong University,
Shanghai 200240, China
e-mail: parker.242@osu.edu

This work provides an analytical solution for the nonlinear vibration of gear pairs that exhibit partial and total contact loss. Partial contact loss is where parts of contact lines lose contact although other parts remain in contact. The gear tooth surface modifications admit an arbitrary combination of profile and lead modifications. Modifications are a source of partial contact loss. The analysis also applies for total contact loss. Unlike models in the literature that are excited by static transmission error or time-varying mesh stiffness, the excitation and the nonlinearity are not a priori specified. Instead, the force-deflection function of the gear pair is provided by an independent source, such as a finite element model or Hertz contact formula. The manipulation of the single-degree-of-freedom oscillator equation of motion yields the excitation and the nonlinearity that arise from Fourier and Taylor series expansions of the force-deflection function. These expansions capture the essential contact behavior that includes tooth profile and lead modifications as well as the bending and shear flexibility of the gear teeth and gear blanks. The method of multiple scales gives the steady-state dynamic response in terms of a frequency-amplitude relation. Comparisons with gear vibration experiments and simulations from the literature that include spur and helical gears with tooth profile and lead modifications verify the method. [DOI: 10.1115/1.4023913]

1 Introduction

Vibration of gear pairs can be considered under the general category of contact vibrations, which also includes vibration of bearings, splines, linkages, and other mechanical connections. This work focuses on nonlinear rotational vibration of gears near resonance speeds. Although gear resonance can be avoided in some constant speed applications, many gears operate over a wide range of speeds where some gear resonances cannot be avoided. In addition, design constraints may prevent changes in the system to move the natural frequencies away from the gear mesh frequency.

In gear applications, the involute tooth surface shape is usually modified slightly. Lead modifications are used to improve misalignment tolerance [1], and profile modifications are used to avoid undesirable edge or corner contact [2]. With or without such tooth modifications, gear vibrations exhibit softening nonlinearity [3–9] near resonance as a result of partial or total contact loss. Partial contact loss is where portions of nominally contacting surfaces lose contact (and other nominally noncontacting portions potentially gain contact) as a result of dynamic motions, profile and lead modifications, or misalignment. Partial contact loss includes reductions in both the profile and face contact ratios. Modifications are the major source of partial contact loss [10]. Although gear systems that exhibit total contact loss have been analyzed, only numerical solutions for the vibration of gears that exhibit partial contact loss are available in the literature; for example Refs. [4,11–15]. This work applies a perturbation method that yields a closed-form solution for nonlinear gear contact vibrations. The method admits spur and helical gears with tooth profile and lead modifications. The solution is compact and exposes the effects of design parameters on the dynamic response. Although harmonic balance can yield closed-form analytical solutions in some nonlinear systems, refined frequency and time discretizations are needed when applying the method to gear contact problems. As a result, the process becomes numerical without expressions showing parameter dependencies of the dynamic response.

The equations of motion for gear vibrations include time-dependent parameters such as periodic variation in mesh stiffness. In many cases, lumped-parameter gear models excited by static transmission error or time-varying mesh stiffness give satisfactory results [6,11,16–21]. A single spring is used to model the gear mesh interface in these works. Velex and Ajmi [21] examine the validity of approximating transmission error as the excitation source. Liu and Parker [22] explore the conditions under which the aforementioned approximations work.

Harmonic balance [23–26] and perturbation methods [27–29] are used when the gear vibration is approximated using a lumped-parameter model. The mesh stiffness formulation in Refs. [24–28] include the periodic fluctuation due to gear tooth engagement/disengagement, while Ref. [23] uses a constant mesh stiffness. The sole source of nonlinearity in the works listed above is total contact loss, a piecewise nonlinearity in which the gear mesh ceases to transmit any force. Gear tooth surface modifications are not included in these works. The modeling in Refs. [22,30] for the dynamic response of multimesh gears differs from the literature listed above because it considers tooth profile modifications and contact loss at each of the individual meshing gear teeth rather than the gear mesh as a whole. In Refs. [22,30], such contact loss is due to linear tooth profile modifications, which is the only type of modification they consider.

Detailed tooth contact models allow dynamic analysis for specified tooth profile and lead modification [3,4,9,31,32]. Such models predict partial contact loss arising from arbitrary tooth surface modifications [4,9,13,15,33,34]. The contact algorithms that allow for partial contact loss, however, are prohibitively complex for analytical methods, and nonlinear dynamic response can only be obtained numerically. Numerical methods give only restricted generalizations about dynamic behavior because they are limited to selected parametric studies. There are no studies in the literature that provide closed-form solutions for the nonlinear vibration of gears when partial contact loss is present.

This work gives closed-form solutions for nonlinear rotational gear vibrations near primary resonance, that is, when the excitation frequency is close to the natural frequency. The solution can accommodate spur and helical gears, and it includes the nonlinear behavior due to partial contact loss and admits arbitrary modifications of the gear tooth surface including profile and lead modifications. The use of a general force-deflection function as an input

[1]Corresponding author.

frees the dynamic equation of motion from the physical gear modeling assumptions and can apply to other contact problems. For gears, the force-deflection function captures the phenomena of partial contact loss, parameter time-dependence, tooth profile and lead modifications, changing number of teeth in contact, changing radius of curvature at contact, and the elastic deformation of the gear blank. With Taylor and Fourier series expansions of this force-deflection function, the equation of motion takes a form that enables use of the method of multiple scales.

2 Mathematical Model

2.1 Equation of Motion. This section considers a single degree-of-freedom equation of motion. The single degree-of-freedom model includes fluctuating mesh stiffness and mesh force nonlinearity. The nonlinear and periodically varying mesh force is represented by a general, time-dependent force-deflection curve that can account for partial contact loss, gear misalignment, tooth surface modifications, varying number of teeth in contact, torque dependence, and total contact loss. Mathematical manipulations of the tooth mesh force-deflection term using Fourier and Taylor series expansion puts the equation of motion in a form suitable for perturbation analysis. These manipulations and the closed-form perturbation approximations for a general mesh force-deflection relationship are what distinguish this work from past studies. The basic gear modeling has been proposed in past research. It is assumed that the force-deflection function and the applied load vary periodically with time. No further assumptions are made at this point.

The equation of motion is

$$m\ddot{x} + c\dot{x} + C(x,t)f(x,t) = F(t) \tag{1}$$

where $F(t)$ is the periodic applied load with period P_F, $f(x,t)$ is the nonlinear, time-dependent, periodic force-deflection function with period P_f, and $C(x,t)$ is the separation function given by

$$C(x,t) = \begin{cases} 0 & \text{if} \quad x < g(t) \\ 1 & \text{if} \quad x \geq g(t) \end{cases} \tag{2}$$

where $g(t)$ is the unloaded $(F(t) = 0)$, quasi-static $(\dot{x} = \ddot{x} = 0)$ transmission error one would measure if the gears are rotated through a gear mesh cycle with zero torque. It satisfies $f(g(t),t) = 0$.

This single degree-of-freedom mechanical oscillator approximates the rotational vibration of gear pairs with the following assumptions. The bearings are assumed to be rigid, allowing a model with only rotational degrees of freedom. This assumption is justified when the natural frequencies of vibration modes with high bearing deformations are sufficiently separated from the natural frequencies of vibration modes with primarily rotational oscillations of the gears.

The force-deflection function $f(x,t)$ is general and there are no restrictions on the type of the elastic deformation that can be included. In gears, the effects include, but are not limited to, Hertz contact deformations at the gear teeth, tooth bending, shear, and gear blank deformations. Because the number of teeth in contact changes with rotation of gears, the force-deflection function is periodic with tooth pass frequency. An important distinction must be made between misaligned gears in the original assembly and dynamic tilting motions that occur during vibrations. We use the term misalignment to refer to a mounting error such that the tooth load is unevenly distributed across the facewidth in its assembled state. Misalignment affects the mesh stiffness and would be reflected in the general force-deflection function, which can be calculated by finite element analysis. Therefore the analysis considers the effects of misalignment. The dynamic tilting motions that would require additional degrees-of-freedom are neglected.

Equation (2) restricts contact loss to single-sided impacts. Elimination of the rigid body motion [19,35] lumps the rotational

inertias of both the pinion (I_p) and gear (I_g) into $m = I_p I_g / \left(I_p r_g^2 + I_g r_p^2 \right)$ in Eq. (1), where r_p and r_g are the pinion and gear base radii, and θ_p and θ_g are the rotational deflections of the pinion and gear. In this case, the load is constant and $F(t) = F = T_p / r_p$ represents the mesh force due to a constant applied torque T_p. Gear vibrations are lightly damped. Damping is reported to be about 2% in Ref. [5], so approximation with viscous damping c is adopted. Assuming well-lubricated gear contact, the tooth friction forces are assumed small with no significant impact on the vibration. With this formulation, $x(t) = \theta_p r_p + \theta_g r_g$ is the dynamic transmission error in Eq. (1), and $x_s = g(t)$ is the unloaded static transmission error.

The force-deflection function $f(x,t)$ is the crucial quantity in this work. For a variety of systems, the force-deflection function can be obtained from experiments, finite element analysis, and analytical contact models. In gears, it is routinely calculated from computational models and readily measured. The force-deflection function, independent of the physical system in question and the method used to obtain it, can be represented by a Taylor series around x_m up to the nth order by

$$f(x,t) = \sum_{i=0}^{n} \frac{1}{i!} \left.\frac{\partial^i f(x,t)}{\partial x^i}\right|_{x=x_m} (x - x_m)^i = \sum_{i=0}^{n} B_i(t)(x - x_m)^i \tag{3}$$

where x_m is the deflection induced by the mean applied load. Averaging the force-deflection function and the applied force over their shortest common period P, x_m is found from

$$\int_0^P F(t)dt = \int_0^P f(x_m,t)dt \tag{4}$$

The Fourier series expansion of $B_i(t)$ in Eq. (3) is

$$B_i(t) = \beta_{i,0} + \sum_{r=1}^{p} \beta_{i,r} \cos(r\xi t - \Phi_{i,r}), \quad i = 0, 1, ..., n \tag{5}$$

where $\xi = 2\pi/P_f$ is the frequency of $f(x,t)$. The Fourier expansion of $F(t)$ is

$$F(t) = F_0 + \sum_{r=1}^{p} F_r \cos(r\zeta t - R_r) \tag{6}$$

where $\zeta = 2\pi/P_F$ is the frequency of $F(t)$. Substitution of $y = x - x_m$, Eqs. (5), and (6) into Eqs. (1) and (2) gives

$$m\ddot{y} + c\dot{y} + C(y,t) \sum_{i=0}^{n} \left[\beta_{i,0} + \sum_{r=1}^{p} \beta_{i,r} \cos(r\xi t - \Phi_{i,r}) \right] y^i$$

$$= F_0 + \sum_{r=1}^{p} F_r \cos(r\zeta t - R_r) \tag{7}$$

$$C(y,t) = \begin{cases} 0 & \text{if} \quad y < -x_m + g(t) \\ 1 & \text{if} \quad y \geq -x_m + g(t) \end{cases} \tag{8}$$

Substitution of $\beta_{0,0} = F_0$, a result of Eqs. (4), (5), and (6) into Eq. (7) eliminates the mean load F_0 under contact, giving

$$m\ddot{y} + c\dot{y} + C(y,t) \sum_{i=1}^{n} \left[\beta_{i,0} + \sum_{r=1}^{p} \beta_{i,r} \cos(r\xi t - \Phi_{i,r}) \right] y^i$$

$$= \sum_{r=1}^{p} F_r \cos(r\zeta t - R_r) - C(y,t) \sum_{r=1}^{p} \beta_{0,r} \cos(r\xi t - \Phi_{0,r})$$

$$- F_0[C(y,t) - 1] \tag{9}$$

so the mean load F_0 acts only when contact is lost.

Fourier expansion of $g(t)$ gives

$$g(t) = g_0 + \sum_{r=1}^{p} g_r \cos(r\xi t - \Psi_r) \qquad (10)$$

The definition $d = x_m - g_0$ and substitution of $T = \omega_n t$, $\omega_n = \sqrt{\beta_{1,0}/m}$, and $y = ud$ give the nondimensional forms of Eqs. (8) and (9) as

$$u'' + 2\mu u' + C(u,T) \sum_{i=1}^{n} \left[\alpha_{i,0} + \sum_{r=1}^{p} \alpha_{i,r} \cos\left(r\Omega_f T - \phi_{i,r}\right) \right] u^i$$

$$= \sum_{r=1}^{p} q_r \cos(r\Omega_F T - \rho_r)$$

$$- C(u,T)\left[\alpha_{0,1} \cos\Omega_f T + \sum_{r=2}^{p} \alpha_{0,r} \cos\left(r\Omega_f T - \phi_{0,r}\right) \right]$$

$$- \alpha_{0,0}[C(u,t) - 1] \qquad (11)$$

$$C(u,T) = \begin{cases} 0 & \text{if} \quad u < -1 + \sum_{r=1}^{p} e_r \cos(r\Omega_f T - \psi_r) \\[2mm] 1 & \text{if} \quad u \ge -1 + \sum_{r=1}^{p} e_r \cos(r\Omega_f T - \psi_r) \end{cases} \qquad (12)$$

where $()' = \mathrm{d}/\mathrm{d}T$, the nondimensional quantities are

$$\Omega_f = \frac{\xi}{\omega_n}, \quad \Omega_F = \frac{\zeta}{\omega_n}, \quad \mu = \frac{c}{2m\omega_n}, \quad q_r = \frac{F_r}{d\beta_{1,0}}(r \ne 0),$$

$$\alpha_{i,r} = \frac{\beta_{i,r} d^{i-1}}{\beta_{1,0}}, \quad e_r = \frac{g_r}{d} \qquad (13)$$

and the phase angles relative to $\Phi_{0,1}$ are $(i = 0, 1, \ldots, n$ and $r = 0, 1, \ldots, p)$

$$\phi_{i,r} = \Phi_{i,r} - \Phi_{0,1}, \quad \rho_r = R_r - \Phi_{0,1}, \quad \psi_r = \Psi_r - \Phi_{0,1} \qquad (14)$$

2.2 Physical Interpretation

2.2.1 Nondimensional Parameters.
The physical interpretation of the important nondimensional parameters are listed below and summarized in Table 1.

(1) The mean load $\alpha_{0,0}$, linear mean stiffness $\alpha_{1,0}$, and nonlinear stiffnesses $\alpha_{i,0}$ $(i > 1)$ come from Taylor expansion of the force-deflection function by Eq. (3). In gears, $\alpha_{0,0}$ represents the constant mesh force, $\alpha_{1,0}$ the linear mesh stiffness, and $\alpha_{i,0}$ $(i > 1)$ the stiffness nonlinearities that include partial contact loss, nonlinear Hertz contact and others.

(2) The excitation harmonics from the force-deflection function, $\alpha_{0,r}$, the harmonics of linear stiffness, $\alpha_{1,r}$, the harmonics of stiffness nonlinearity $\alpha_{i,r}$ $(i > 1)$ $r > 0$ and associated phase angles $\phi_{i,r}$ come from Fourier expansion of the Taylor coefficients $B_i(t)$ by Eq. (5). They exist in gears due to periodic engagement/disengagement of the gear teeth. The quantity $\alpha_{0,r}$ excites the dynamics. It is close to what is called the "static transmission error excitation" for unmodified gears. The $\alpha_{1,r}$ represents the periodic change in the linear mesh stiffness. The periodicity of the stiffness nonlinearity, that is, changes in the strength of nonlinearity as the gear teeth engage/disengage, is contained in $\alpha_{i,r}$, $(i > 1)$.

(3) The harmonics of the external excitation q_r and associated phase angles ρ_r come from Fourier expansion of the applied force $F(t)$ by Eq. (6). When the applied torque is constant, $q_r = 0$, and the first harmonic of the fluctuating torque is reflected in q_1 that, if exists, further excites the system.

(4) The harmonics of the unloaded deflection e_r and associated phase angles ψ_r come from Fourier expansion of the unloaded deflection $g(t)$ by Eq. (10) and represent the time-dependent unloaded transmission error.

2.2.2 Partial Contact Loss.
Partial contact loss occurs when portions of nominal gear contact lines lose contact while the other parts are still in contact [9,10]. This contrasts with total contact loss, where the gear mesh ceases to transmit any force. Gear

Table 1 Summary of nondimensional parameters and their physical interpretation for gear vibrations

Parameter	Definition	Source in gears
$\alpha_{0,0}$	Mean applied load Acts only when contact is lost	Constant mesh force
$\alpha_{0,r}$ $r > 0$	Harmonics of parametric excitation from force-deflection function	Periodic change in the number of contacting teeth
$\alpha_{1,0}$	Linear mean stiffness	Linearized gear mesh stiffness at the operating torque
$\alpha_{1,r}$ $r > 0$	Harmonics of linear time dependent stiffness	Periodic change in the number of contacting teeth
$\alpha_{i,0}$	Nonlinear stiffness	Partial contact loss nonlinear Hertz contact, etc.
$\alpha_{i,r}$ $r > 0$	Harmonics of time dependent nonlinear stiffness	Periodic changes in partial contact loss, Hertz contact, etc.
e_r	Harmonics of unloaded deflection	Fluctuating unloaded transmission error
q_r	Harmonics of external excitation	Pulsations in applied torque (not analyzed in this work)
d	Mean deflection	Mean loaded transmission error
Ω_f	Parametric excitation frequency of $f(x,t)$	Periodic change in the number of contacting teeth
Ω_F	External excitation frequency of $F(t)$	Pulsations in applied torque (not analyzed in this work)

(a)   (b)
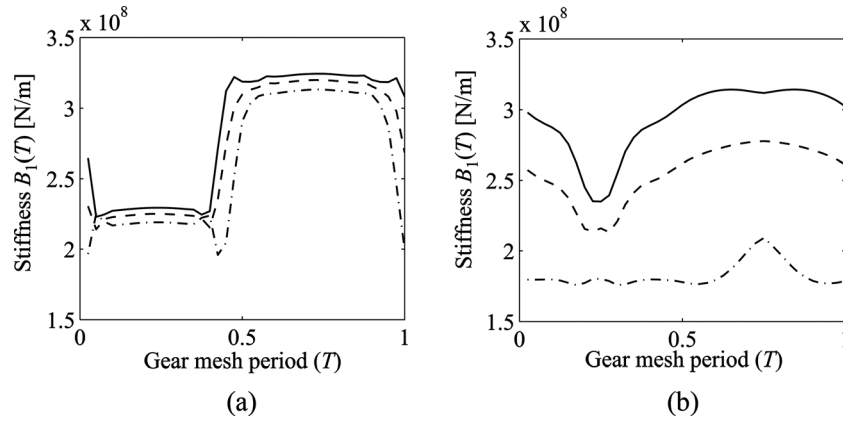
Fig. 1 Dimensional gear mesh stiffness at 50 Nm (dashed-dotted line), 150 Nm (dashed line), and 250 Nm (solid line) using finite element analysis. (*a*) Unmodified spur gear pair from [36] (*ICR* = 1.37). (*b*) Modified spur gear pair from [5] (tip relief starts at 22.2 deg).


(a)   (b)
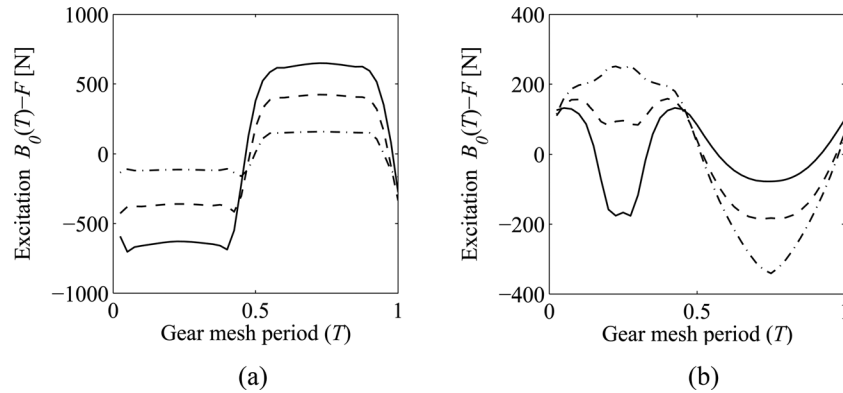
Fig. 2 Dimensional mean-removed excitation levels from the gears in Fig. 1 at 50 Nm (dashed-dotted line), 150 Nm (dashed line), and 250 Nm (solid line) using finite element analysis. (*a*) Unmodified spur gear pair. (*b*) Modified spur gear pair.

vibrations combined with tooth profile and lead modifications cause partial contact loss. Partial contact loss depends heavily on applied torque. The mesh stiffness of modified gears, which depends on the total length of the contacting lines, changes with applied torque. Figure 1 demonstrates this dependence by comparing the dimensional mesh stiffness of unmodified and modified gears. The modified gears depend heavily on torque; the unmodified gears do not. This dependence of stiffness on torque is a source of nonlinearity, and it results from partial contact loss. The parameters $\alpha_{i,r}$ and $\phi_{i,r}$ for $i > 1$ incorporate partial contact loss, and any other nonlinearity present in the force-deflection function, into the equation of motion. Static finite element analysis at many points in a tooth mesh cycle is one effective way to compute the force-deflection function considering partial contact loss and Hertz contact nonlinearity. Commercial software can do this accurately.

2.2.3 Independence of Total Contact Loss From Applied Torque. The analysis helps explain the observation in Refs. [6,22,30,37,38] that, for steady torque systems that do not involve gear rattle, increasing the applied torque does not reduce the occurrence of contact loss near primary resonance in unmodified gears; that is, if contact loss occurs at one torque, it will occur at any other torque. Once contact loss occurs, however, the extent of contact loss and the nature of the nonlinear response will depend on applied torque.

To explain, Fig. 2 shows dimensional, mean-removed excitations from an unmodified and a modified gear pair. The dimensional mean removed excitation $B_0(t) - F_0$ and the mean deflection x_m for unmodified gears are almost directly proportional to the applied torque. The modified gears show no such proportionality. The first harmonic of the nondimensional excitation $\alpha_{0,1}$
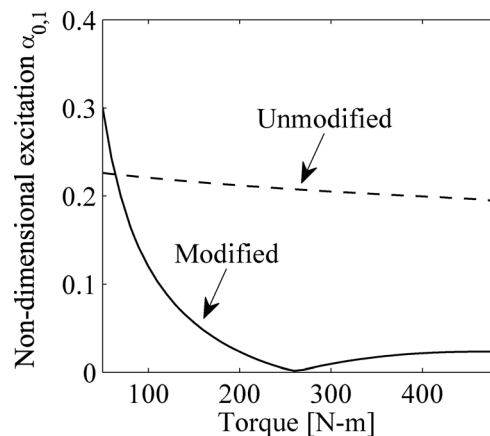
Fig. 3 The first harmonic of nondimensional excitation from the unmodified and modified gears with varying applied torque. The gears are the same as in Fig. 1.

is the dominant driver of vibrations near primary resonance. This quantity from the unmodified and modified gear pairs is shown in Fig. 3. Changing the applied torque does not change the first harmonic of the excitation for the unmodified gear pair much, but it dramatically changes this quantity for the modified gear pair. In other words, the first harmonic of the excitation is sensitive to torque for modified gears, but insensitive to torque for unmodified gears. Because the first harmonic of the nondimensional excitation $\alpha_{0,1}$ from unmodified gears is similar for any applied torque, the

applied torque has no effect upon the occurrence of contact loss. This mathematical explanation translates into a physical explanation as follows. In unmodified gears, a higher torque nearly linearly increases both: (a) the excitation and so the vibration amplitude, and (b) the threshold of vibration amplitude needed to trigger contact loss. In summary

(1) For unmodified gears, the occurrence of contact loss is independent of the applied torque.
(2) For modified gears, the occurrence of contact loss depends on the applied torque.
(3) Once contact loss starts to occur, the vibrations depend on applied torque. The amplitude of applied torque affects the duration of separation in a mesh period, and the vibration amplitude.

3 Analysis Method

3.1 Dynamic Response Near Primary Resonance. This section presents approximate analytical solutions of Eqs. (11) and (12) near the primary resonance region using the method of multiple scales. To unify the analysis, we consider that parametric and external excitations are both present and their frequencies are equal and close to the natural frequency, $\Omega = \Omega_f = \Omega_F \approx 1$. The reason for setting $\Omega_f = \Omega_F$ is to keep the length of the closed-form solution to a minimum and to allow for periodic external torque excitation near resonant speed; thus there is no reason to consider $\Omega_f \neq \Omega_F$. Following Ref. [39] to expand u, T, and the forcing frequency Ω near the primary resonance gives

$$u(T,\varepsilon) = u_0(T_0,T_1,T_2) + \varepsilon u_1(T_0,T_1,T_2) + \varepsilon^2 u_2(T_0,T_1,T_2)$$
$$T_n = \varepsilon^n T, \quad \Omega = 1 + \sigma = 1 + \varepsilon \hat{\sigma} \tag{15}$$

The small parameter ε is a detuning parameter such that the excitation frequency is close to the natural frequency. The separation function in Eq. (12) is rewritten as $C = 1 + H$ where

$$H(u,t) = \frac{1}{2}\text{sgn}\left[u + 1 - \sum_{r=1}^{p} e_r \cos(rT - \psi_r)\right] - \frac{1}{2} \tag{16}$$

This allows p contact losses per period. Fourier expansion of $H(u,t)$ is admissible because, like $u(t)$, it has period 2π, giving

$$H = \Delta_0 + \sum_{r=1}^{N} \Delta_r \cos(rT_0 - \nu_r) \tag{17}$$

The quantities Δ_0 and Δ_r depend on $u(t)$ and are not yet known. Arbitrarily, many harmonics can be used to represent the separation function H, but N must not be less than the number of contact losses per period, $N \geq p$. These steps turn contact loss into a form manageable by the method of multiple scales [22,30,40,41].

The $O(\varepsilon)$ parameters are

$$\alpha_{0,1} = \varepsilon\hat{\alpha}_{0,1}, \quad \alpha_{2,0} = \varepsilon\hat{\alpha}_{2,0}, \quad \alpha_{3,0} = \varepsilon\hat{\alpha}_{3,0}, \quad q_1 = \varepsilon\hat{q}_1, \quad \mu = \varepsilon\hat{\mu},$$
$$\sigma = \varepsilon\hat{\sigma}, \quad \Delta_0 = \varepsilon\hat{\Delta}_0 \tag{18}$$

These orderings reflect the assumption that the nonlinearities, forcing, and damping are small. The mean value Δ_0 of the separation function H is ordered by assuming that the duration of contact loss is small compared to the period of vibration. Furthermore, all harmonics are assumed one order smaller than the corresponding mean values. This gives the $O(\varepsilon^2)$ parameters as

$$\alpha_{2,1} = \varepsilon^2\hat{\alpha}_{2,1}, \quad \Delta_1 = \varepsilon^2\hat{\Delta}_1, \quad \Delta_2 = \varepsilon^2\hat{\Delta}_2 \tag{19}$$

We consider up to the third order polynomial approximation of the nonlinear force-deflection function, that is, $\alpha_{i,r} \approx 0$ for $i \geq 4$, and the first harmonic of the periodically varying force-deflection function, that is, $\alpha_{i,r} \approx 0$ for $r \geq 2$. Parametric instability due to the first harmonic of the linear stiffness variation $\alpha_{1,1}$ is possible, but this needs to be treated separately. The third and higher

harmonics of the separation function (Δ_r for $r \geq 3$) and excitations $\alpha_{0,r}$ and q_r for $r \geq 2$ do not contribute to the solution, so they are excluded from subsequent equations for brevity.

Substitution of Eq. (15) into Eq. (11) and combining like orders of ε gives the perturbation equations

$$D_0^2 u_0 + u_0 = 0 \tag{20}$$

$$D_0^2 u_1 + u_1 = -2D_0 D_1 u_0 - \hat{\alpha}_{2,0} u_0^2 - \hat{\alpha}_{3,0} u_0^3 - 2\hat{\mu} D_0 u_0$$
$$- \hat{\Delta}_0(u_0 + \alpha_{0,0}) - \frac{\hat{\alpha}_{0,1}}{2}\left(e^{iT_0} + e^{-iT_0}\right)$$
$$+ \frac{\hat{q}_1}{2}\left[e^{i(T_0-\rho_1)} + e^{-i(T_0-\rho_1)}\right] \tag{21}$$

$$D_0^2 u_2 + u_2 = -2\hat{\mu}(D_1 u_0 + D_0 u_1) - 2D_0 D_1 u_1 - 2D_0 D_2 u_0$$
$$- D_1^2 u_0 - (u_1 + \hat{\alpha}_{2,0}u_0^2 + \hat{\alpha}_{3,0}u_0^3)\hat{\Delta}_0 - 2\hat{\alpha}_{2,0}u_0 u_1$$
$$- 3\hat{\alpha}_{3,0}u_0^2 u_1 - \frac{\hat{\alpha}_{0,1}\hat{\Delta}_0}{2}\left(e^{iT_0} + e^{-iT_0}\right)$$
$$- \frac{(\alpha_{0,0} + u_0)\hat{\Delta}_1}{2}\left[e^{i(T_0-\nu_1)} + e^{-i(T_0-\nu_1)}\right]$$
$$- \frac{(\alpha_{0,0} + u_0)\hat{\Delta}_2}{2}\left[e^{i(2T_0-\nu_2)} + e^{-i(2T_0-\nu_2)}\right]$$
$$- \frac{\hat{\alpha}_{2,1}u_0^2}{2}\left[e^{i(T_0-\phi_{2,1})} + e^{-i(T_0-\phi_{2,1})}\right] \tag{22}$$

where $D_i = \partial/\partial T_i$. The general solution of Eq. (20) is

$$u_0 = A(T_1,T_2)e^{iT_0} + \bar{A}(T_1,T_2)e^{-iT_0} \tag{23}$$

Substitution of Eq. (23) into the first order Eq. (21) yields secular terms that must be eliminated for u_0 to be periodic, giving the condition

$$2iD_1 A + A\left[2i\hat{\mu} + \hat{\Delta}_0 + 3\hat{\alpha}_{3,0}A^2\bar{A}\right] + \frac{\hat{\alpha}_{0,1}}{2}e^{i\hat{\sigma}T_1} - \frac{\hat{q}_1}{2}e^{i(\hat{\sigma}T_1-\rho_1)} = 0 \tag{24}$$

Transforming to polar coordinates by setting $A = 1/2ae^{i\beta}$, $\beta = \hat{\sigma}T_1 - \gamma$, with $a, \gamma \in \mathbb{R}$ gives the real and imaginary parts of Eq. (24) as

$$aD_1\gamma = a\hat{\sigma} - \frac{1}{2}a\hat{\Delta}_0 - \frac{3}{8}\hat{\alpha}_{3,0}a^3 - \frac{1}{2}\hat{\alpha}_{0,1}\cos\gamma + \frac{1}{2}\hat{q}_1\cos(\gamma-\rho_1)$$
$$D_1 a = -\hat{\mu}a - \frac{\hat{\alpha}_{0,1}}{2}\sin\gamma + \frac{1}{2}\hat{q}_1\sin(\gamma-\rho_1) \tag{25}$$

3.1.1 First Order Perturbation. If the process is terminated at the first order perturbation, only Eq. (25) is considered. The steady state solutions of Eq. (23) result from $D_1 a = 0$, $D_1\gamma = 0$ in Eq. (25). This gives, after use of Eq. (18), the frequency-amplitude relation cast in terms of the original parameters independent of ε as

$$a\sigma - \frac{1}{2}a\Delta_0 - \frac{3}{8}\alpha_{3,0}a^3 - \frac{1}{2}\alpha_{0,1}\cos\gamma + \frac{1}{2}q_1\cos(\gamma-\rho_1) = 0$$
$$- \mu a - \frac{1}{2}\alpha_{0,1}\sin\gamma + \frac{1}{2}q_1\sin(\gamma-\rho_1) = 0 \tag{26}$$

These two equations can be combined by eliminating γ, giving

$$\mu^2 a^2 + \left(a\sigma - \frac{1}{2}\Delta_0 a - \frac{3}{8}\alpha_{3,0}a^3\right)^2 - \frac{\alpha_{0,1}^2 + q_1^2}{4} + \frac{\alpha_{0,1}q_1}{2}\cos\rho_1 = 0 \tag{27}$$

Many parameters ($\alpha_{0,0}$, $\alpha_{2,0}$, $\alpha_{2,1}$, $\phi_{2,1}$, Δ_1, Δ_2, ν_1, and ν_2) do not appear in Eq. (26) and only contribute through the second order perturbation. After calculation of the general solution of Eq. (21), the approximate solution is constructed from $u = u_0 + \varepsilon u_1 + O(\varepsilon^2)$, giving

$$u = a\cos(T_0 - \gamma) + \frac{\alpha_{2,0}a^2}{2}\left[\frac{1}{3}\cos(2T_0 - 2\gamma) - 1\right]$$
$$+ \frac{\alpha_{3,0}a^3}{32}\cos(3T_0 - 3\gamma) - \alpha_{0,0}\Delta_0 + O(\varepsilon^2) \qquad (28)$$

3.1.2 Second Order Perturbation.
Proceeding to the second order perturbation, substitution of Eqs. (28) into (22) yields secular terms that need to be eliminated for u_1 to have a periodic solution, giving the condition

$$D_1^2 A + 2iD_2 A + 2\mu D_1 A - \frac{10}{3}\hat{\alpha}_{2,0}^2 A\bar{A} + \frac{3}{8}\hat{\alpha}_{3,0}^2 A^3\bar{A}^2 + \hat{\Delta}_0\left(\frac{\hat{\alpha}_{0,1}}{2}e^{i\hat{\sigma}T_1} - 2A\alpha_{0,0}\hat{\alpha}_{2,0} + 3A^2\bar{A}\hat{\alpha}_{3,0}\right)$$
$$+ \frac{\alpha_{0,0}\hat{\Delta}_1}{2}e^{i(\sigma T_1 - \nu_1)} + \frac{A^2\hat{\alpha}_{2,1}}{2}e^{-i(\hat{\sigma}T_1 - \phi_{2,1})} + \frac{\bar{A}\hat{\Delta}_2}{2}e^{i(2\hat{\sigma}T_1 - \nu_2)} + A\bar{A}\hat{\alpha}_{2,1}e^{i(\hat{\sigma}T_1 - \phi_{2,1})} = 0 \qquad (29)$$

Substitution of $D_1 A$ from Eq. (24) into Eq. (29) and use of the polar coordinates $a(T_1, T_2)$ and $\gamma(T_1, T_2)$ give the real and imaginary parts of Eq. (29) as

$$aD_2\gamma = \left[\hat{\alpha}_{0,1}\cos\gamma - \hat{q}_1\cos(\gamma - \rho_1)\right]\left(\frac{3}{32}\hat{\alpha}_{3,0}a^2 + \frac{1}{4}\hat{\sigma}\right) - \frac{3}{8}\hat{\Delta}_0\hat{\alpha}_{0,1}\cos\gamma + \frac{1}{4}\hat{\mu}\hat{\alpha}_{0,1}\sin\gamma$$
$$- \frac{1}{4}\hat{\mu}\hat{q}_1\sin(\gamma - \rho_1) - \frac{1}{2}\alpha_{0,0}\hat{\Delta}_1\cos(\nu_1 - \gamma) - \frac{1}{4}\hat{\Delta}_2 a\cos(\nu_2 - 2\gamma) - \frac{3}{8}\hat{\alpha}_{2,1}a^2\cos(\Phi_{2,1} - \gamma)$$
$$+ \frac{1}{8}\hat{\Delta}_0^2 a - \frac{3}{16}\hat{\alpha}_{3,0}\hat{\Delta}_0 a^3 + \frac{1}{2}\hat{\mu}^2 a + \frac{15}{256}a^5\hat{\alpha}_{3,0}^2 + a\hat{\alpha}_{2,0}\alpha_{0,0}\hat{\Delta}_0 + \frac{5}{12}a^3\hat{\alpha}_{2,0}^2$$

$$D_2 a = \left[\hat{\alpha}_{0,1}\sin\gamma - \hat{q}_1\sin(\gamma - \rho_1)\right]\left(\frac{9}{32}\hat{\alpha}_{3,0}a^2 + \frac{1}{4}\hat{\sigma}\right) - \frac{3}{8}\hat{\Delta}_0\hat{\alpha}_{0,1}\sin\gamma - \frac{1}{4}\hat{\mu}\hat{\alpha}_{0,1}\cos\gamma$$
$$+ \frac{1}{4}\hat{\mu}\hat{q}_1\cos(\gamma - \rho_1) + \frac{3}{8}\hat{\mu}\hat{\alpha}_{3,0}a^3 + \frac{1}{2}\alpha_{0,0}\hat{\Delta}_1\sin(\nu_1 - \gamma)$$
$$+ \frac{1}{4}\hat{\Delta}_2 a\sin(\nu_2 - 2\gamma) + \frac{1}{8}\hat{\alpha}_{2,1}a^2\sin(\Phi_{2,1} - \gamma) \qquad (30)$$

Steady-state vibration requires $D_1 a = D_1\gamma = 0$ in Eq. (25) and $D_2 a = D_2\gamma = 0$ in Eq. (30). Combination of the real and imaginary parts of Eqs. (25) and (30) according to the reconstitution method [41,42], substitution of $D_1 a = D_1\gamma = 0$ into Eq. (25) and $D_2 a = D_2\gamma = 0$ into Eq. (30), and use of Eqs. (18) and (19) in that sequence give the frequency-amplitude relations

$$a\sigma - \frac{\Delta_0}{2}a - \frac{3\alpha_{3,0}a^3}{8} - \frac{\alpha_{0,1}}{2}\cos\gamma + \frac{q_1}{2}\cos(\gamma - \rho_1) + \left\{\frac{1}{4}\mu\alpha_{0,1}\sin\gamma - \frac{1}{4}\mu q_1\sin(\gamma - \rho_1) + \left[\alpha_{0,1}\cos\gamma - q_1\cos(\gamma - \rho_1)\right]\left(\frac{3}{32}\alpha_{3,0}a^2 + \frac{1}{4}\sigma\right)\right.$$
$$- \frac{3}{8}\Delta_0\alpha_{0,1}\cos\gamma - \frac{1}{2}\alpha_{0,0}\Delta_1\cos(\nu_1 - \gamma) - \frac{1}{4}\Delta_2 a\cos(\nu_2 - 2\gamma) - \frac{3}{8}\alpha_{2,1}a^2\cos(\Phi_{2,1} - \gamma) + \frac{1}{8}\Delta_0^2 a - \frac{3}{16}\alpha_{3,0}\Delta_0 a^3 + \frac{1}{2}\mu^2 a + \frac{15}{256}a^5\alpha_{3,0}^2$$
$$\left. + a\alpha_{2,0}\alpha_{0,0}\Delta_0 + \frac{5}{12}a^3\alpha_{2,0}^2\right\} = 0 - \mu a - \frac{1}{2}\alpha_{0,1}\sin\gamma + \frac{1}{2}q_1\sin(\gamma - \rho_1) + \left\{-\frac{1}{4}\mu\alpha_{0,1}\cos\gamma + \frac{1}{4}\mu q_1\cos(\gamma - \rho_1)\right.$$
$$+ \left[\alpha_{0,1}\sin\gamma - q_1\sin(\gamma - \rho_1)\right]\left(\frac{9}{32}\alpha_{3,0}a^2 + \frac{1}{4}\sigma\right) - \frac{3}{8}\Delta_0\alpha_{0,1}\sin\gamma + \frac{3}{8}\mu\alpha_{3,0}a^3 + \frac{1}{2}\alpha_{0,0}\Delta_1\sin(\nu_1 - \gamma) + \frac{1}{4}\Delta_2 a\sin(\nu_2 - 2\gamma)$$
$$\left. + \frac{1}{8}\alpha_{2,1}a^2\sin(\Phi_{2,1} - \gamma)\right\} = 0 \qquad (31)$$

from which a and γ can be solved. The expressions outside of the brackets are the first order perturbation solution, and the expressions inside the brackets are the second order corrections.

3.1.3 Separation.
The quantities Δ_r and ν_r in Eq. (17) are found using the separation instants T_i. These separation instants are solved by substitution of u from Eq. (28) into Eq. (16) for $H = -1$ (i.e., $C = 0$). For arbitrarily many contact losses per period p, the solutions T_i, $i = 1, ..., 2p + 1$, mark the instants when contact is lost or re-established. Let H_i denote whether there is contact ($H_i = 0$) or not ($H_i = -1$) when $T_i \leq T < T_{i+1}$. The Fourier coefficients and phase angles of the separation function H in Eq. (17) are then

$$\Delta_0 = \frac{1}{2\pi}\sum_{i=1}^{2p}(T_{i+1} - T_i)H_i \qquad (32)$$

$$\Delta_r = \sqrt{\Delta_{r,a}^2 + \Delta_{r,b}^2}, \quad \nu_r = \tan^{-1}(\Delta_{r,b}, \Delta_{r,a}), r = 1, ..., N$$
$$\Delta_{r,a} = \frac{1}{r\pi}\sum_{i=1}^{2p}(\sin rT_{i+1} - \sin rT_i)H_i, \qquad (33)$$
$$\Delta_{r,b} = -\frac{1}{r\pi}\sum_{i=1}^{2p}(\cos rT_{i+1} - \cos rT_i)H_i, \quad r = 1, ..., N$$

The perturbation solution considers a maximum of $N = 2$ because harmonics of H higher than the second, i.e., Δ_r for $r > 2$ in Eq. (17), do not yield secular terms. This limits contact loss to twice-per-period because $N \geq p$. Even when the contact loss is limited to twice-per-period, finding the separation instants T_i requires solving Eq. (16) for $p = 2$. Finding a closed-form solution is not feasible unless: (1) contact loss occurs once per period ($p = 1$), and (2) the mean change in solution u due to contact loss does not

affect when contact loss starts and ends ($\alpha_{0,0}\Delta_0 = 0$). Adopting these assumptions gives the closed-form expressions

$$\Delta_0 = -1 + \frac{\tau}{\pi}, \quad \Delta_r = \frac{2}{r\pi}\sin r\tau$$

$$\nu_r = r\tan^{-1}(-a\sin\gamma + e_1\sin\psi_1, a\cos\gamma - e_1\cos\psi_1), r = 1, 2 \tag{34}$$

$$\tau = \cos^{-1}\left(\frac{-1 + \alpha_{2,0}a/2}{\sqrt{(a\cos\gamma - e_1\cos\psi_1)^2 + (a\sin\gamma - e_1\sin\psi_1)^2}}\right) \tag{35}$$

The numerical solution for Δ_0, Δ_r, and ν_r using Eqs. (32) and (33) is computationally demanding. To save computation when analyzing a system with the second order perturbation solution Eq. (31), we use a coarse frequency resolution across the frequency range

of interest to confirm that contact loss occurs once per period using numerical solutions of Eqs. (32) and (33). Once confirmed, the analytical expressions in Eqs. (34) and (35) are used. The analytical expressions in Eqs. (34) and (35) and numerical solution of Eqs. (32) and (33) give almost identical results for the cases analyzed in this work, so the presented results use the analytical expressions. This comparison justifies the assumption of only one instance of contact loss per mesh period for the current system. For a set of parameters with even stronger nonlinearity at resonance, the perturbation solution assumptions must be re-evaluated to confirm their suitability.

The vibration amplitude and frequency at the onset of total contact loss can be found from the foregoing analytical solution. Just before the onset of total contact loss, the mean value of the separation function and its harmonics are zero and $\Delta_0 = \Delta_r = 0$ in Eq. (34). This gives $\tau = \pi$. Substitution of $\tau = \pi$ into Eq. (35) gives the amplitude at the onset of total contact loss as

$$a = \frac{4e_1\cos(\gamma - \psi_1) - 2\alpha_{2,0} \pm 2\sqrt{e_1^2\alpha_{2,0}^2 + 4 - 4e_1^2\sin^2(\gamma - \psi_1) - 4e_1\alpha_{2,0}\cos(\gamma - \psi_1)}}{4 - \alpha_{2,0}^2} \tag{36}$$

Substitution of a from Eq. (36) and $\Delta_0 = \Delta_r = 0$ into Eq. (31) gives the frequency σ and the phase γ at the onset of total contact loss. The closed-form solution is lengthy using the second order perturbation solution, but a compact expression can be obtained using the first order perturbation solution. The first order does not consider quadratic nonlinearity and unloaded fluctuations (they do not yield secular terms), so $\alpha_{2,0} = e_1 = 0$. Subsequently, Eq. (36) reveals that $a = 1$ initiates total contact loss. Substitution of $a = 1$ and $\Delta_0 = 0$ into Eq. (27) gives the two frequencies where total contact loss starts as

$$\sigma = \pm\sqrt{\frac{\alpha_{0,1}^2 + q_1^2}{4} - \mu^2 - \frac{\alpha_{0,1}q_1}{2}\cos\rho_1 + \frac{3}{8}\alpha_{3,0}} \tag{37}$$

3.1.4 Key Points from the Analytical Solution

(1) The first order perturbation gives the frequency amplitude relation by Eq. (27). It considers only the cubic nonlinearity $\alpha_{3,0}$ and the mean reduction of stiffness due to total contact loss Δ_0.

(2) The second order perturbation solution gives the frequency amplitude relation by Eq. (31). It considers quadratic nonlinearities ($\alpha_{2,0}$, $\alpha_{2,1}$, $\phi_{2,1}$), and cubic nonlinearity ($\alpha_{3,0}$). The mean value of the separation (Δ_0) and its first two harmonics (Δ_1, Δ_2) with associated phase angles (ν_1, ν_2) contribute. These quantities account for total contact loss.

(3) The mean value (Δ_0) and the first two harmonics (Δ_1, Δ_2) of the separation function and their phase angles (ν_1, ν_2) are found from the perturbation equations numerically from Eqs. (32) and (33) or analytically from Eqs. (34), (35) when contact loss is limited to once per period ($p = 1$). Both harmonics are crucial for an accurate response as the upcoming results will show.

(4) When the expression inside $\cos^{-1}$ in Eq. (35) is not in the range $(-1, 1)$, total contact loss does not occur. The amplitude and frequency at onset of contact loss is analytically given by Eq. (37) from the first order perturbation. The second order approximation of the amplitude at onset of contact loss is found from Eq. (36) and the frequencies can be solved by substitution of that amplitude into Eq. (31).

3.2 Stability. The solution of Eq. (31) can give one or three solutions for a given frequency. When more than one solution is

possible, only the stable solutions would be observed in practice or calculated by numerical integration. The stability of a solution is found by linearizing Eqs. (25) and (30) about a stationary point (a, γ). This yields the matrix form

$$\frac{d}{dT}\begin{pmatrix} a \\ \gamma \end{pmatrix} = \mathbf{J}\begin{pmatrix} a \\ \gamma \end{pmatrix} \tag{38}$$

where the matrix $\mathbf{J}$ denotes the Jacobian. The solution is unstable if any eigenvalues of $\mathbf{J}$ have a positive real part. The algebraic expression for $\mathbf{J}$ is prohibitively long and provides no practical insight. For these reasons, the stability is found numerically from the Jacobian matrix $\mathbf{J}$ at the stationary points.

4 Results

In this section, dynamic response of the equation of motion Eq. (11) obtained using the perturbation solution in Eq. (28) is compared with gear vibration experiments from the literature, numerical integration, and the linearized solution. The first order perturbation solution is found from Eq. (27), and the second order perturbation solution is found from Eq. (31).

4.1 Key Regions in Dynamic Response and Comparison With Numerical Solution. Independent of the physical system analyzed, there are four possible distinct regions in the nonlinear response. To investigate the characteristics of these four regions, time domain numerical integration and the second order perturbation solution of an example system are shown in Fig. 4. The linear time-invariant solution (only linear stiffness and external excitation exist, $\alpha_{1,0}, \alpha_{0,1} \neq 0$) is plotted to provide a comparison:

Region 1. The linear and nonlinear solutions give almost identical responses. The response is relatively small. There is no contact loss, and nonlinear terms negligibly affect the response.

Region 2. The nonlinear solution deviates significantly from the linear solution as the vibration amplitude grows. This region does not exist, i.e., becomes identical to region 1, if $\alpha_{2,0} = 0$ and $\alpha_{3,0} = 0$. Although the contact is maintained, this region represents partial contact loss in physical systems, where the nonlinearities are due to a reduction in instantaneous dynamic stiffness.
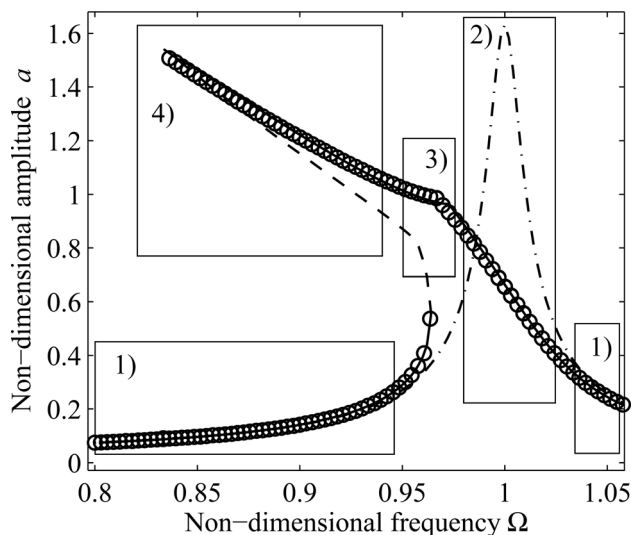
Fig. 4 Dynamic response of equation of motion (Eqs. (11)–(12)) using second order perturbation and numerical integration. Parameters are: $\alpha_{0,1} = 2/75$, $\alpha_{0,0} = 2/3$, $\alpha_{2,0} = 1/4$, $\alpha_{3,0} = -1/24$, $e_1 = 0.1$, $\psi_1 = 0$, $\alpha_{2,1} = 0$, $\mu = 0.0082$. Important regions of solutions are marked with (1) through (4). (Stable perturbation solution: solid line, unstable perturbation solution: dashed line, numerical integration: circles, linear solution: dashed-dotted line.)

The nonlinear terms $\alpha_{2,0}$, $\alpha_{3,0}$, and the time-dependence $\alpha_{2,1}$, $\phi_{2,1}$ dominate the response.

Region 3. Total contact loss, manifest from the kink in the response at $\Omega = 0.97$, starts in this region. Here $C = 0$. The vibration amplitude a and the frequency of excitation Ω at which total contact loss starts is given by Eq. (36). It depends on the quadratic nonlinearity, the fluctuation in the unloaded deflection e_1, and the relative phase angle $\gamma - \psi_1$.

Region 4. Total contact loss occurs. The solution is dominated by the mean reduction in stiffness Δ_0 due to separation, the first two harmonics of the separation function Δ_1, Δ_2, their phase angles ν_1, ν_2, and the mean load $\alpha_{0,0}$. The agreement between the numerical and perturbation solution is excellent, justifying the assumptions in the perturbation solution. The nonlinearities are stronger if the periods of separation become long, which would degrade the agreement somewhat as shown in Ref. [37] for a simpler tooth mesh contact model in planetary gears.

4.2 Gear Vibrations

4.2.1 Computational Results. Computational dynamic response of a helical gear pair is obtained using the contact algorithm in Refs. [9,10]. That model has been successfully compared against experiments and a specialized finite element/contact mechanics model of gear dynamics. Some elastic behaviors, such as corner contact, radius of curvature effects, buttressing effects, and the coupling between the deflections of adjacent teeth, are neglected in this contact algorithm.

The gear parameters, which are from [9], are listed in Table 2. The nondimensional parameters are given in Table 3.

The dynamic response of the helical gear pair with profile and lead modifications and the force-deflection function shown in Fig. 5 is plotted in Fig. 6. The computational dynamic response and perturbation solution agree throughout most of the operating frequencies. There is a clear difference between the linear and the nonlinear response. Region 2 of Fig. 4 identifies this type of response. Physically, this difference is attributed to partial contact loss, where some portions of the nominal contact lines separate while the gear mesh as a whole is still engaged. The perturbation

Table 2 Physical parameters of the helical gears analyzed in Fig. 6

Parameter	Pinion	Common	Gear
Number of teeth	27		35
Transverse module (mm)	3		3
Base helix angle (deg)		28.08	
Transverse operating pressure angle (deg)		24.60	
Facewidth (mm)	20.00		20.00
Center distance (mm)		88.90	
Profile crown (μm)	0		10
Lead crown (μm)	0		10

Table 3 Parameters of the analyzed gears in Figs. 6, 9, 10, and 11

|	Figure 6	Figure 9	Figure 10	Figure 11
$\alpha_{0,0}$	0.727	0.727	0.716	0.714
$\alpha_{0,1}$	0.069	0.181	0.061	0.058
$\alpha_{2,0}$	0.209	0.213	0.197	0.202
$\alpha_{2,1}$	0.313	0.212	0.118	0.069
$\alpha_{3,0}$	−0.037	−0.034	−0.074	−0.074
$\phi_{2,1}$ (rad)	−2.891	−3.203	−3.228	−0.230
e_1	0.167	0.302	0.185	0.038
ψ_1 (rad)	−3.293	−3.124	−3.124	0.037
μ	0.030	0.050	0.016	0.028
d (μm)	4.350	5.516	9.005	9.201
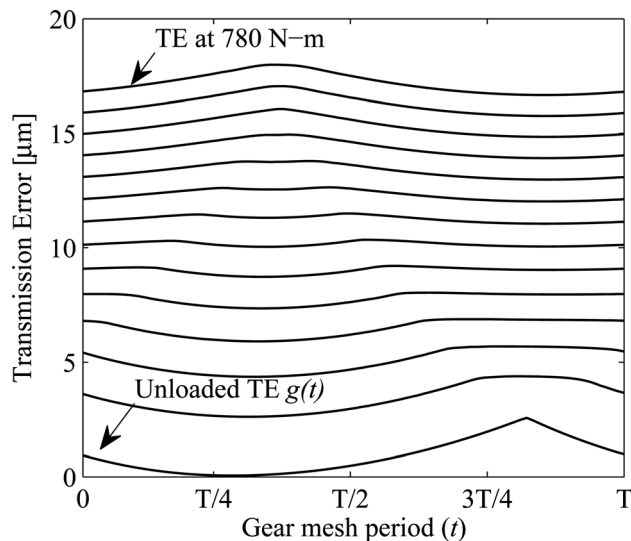
Fig. 5 Force-deflection function $f(x,t)$ of a helical gear pair obtained by the method of Ref. [9]. Tooth surface modifications are: quadratic profile tip and root crown of 10μm and lead crown of 10μm on the gear.

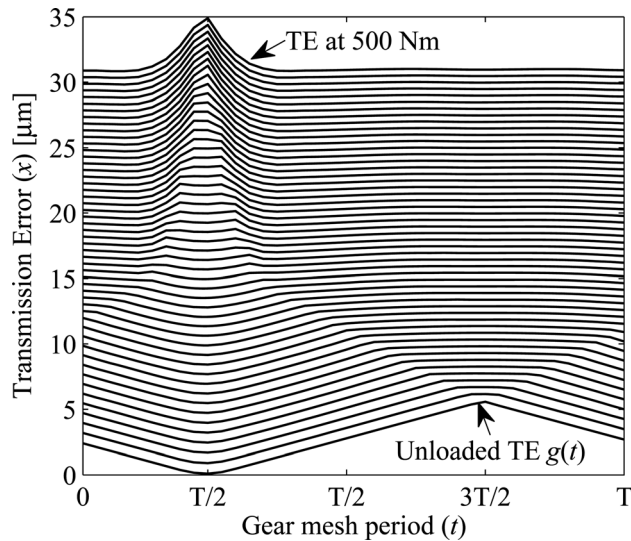solution predicts the nonlinear dynamics arising from partial contact loss.

The investigation of practical gear vibration raises the question of whether all the nonlinear terms ($\alpha_{2,0}$, $\alpha_{3,0}$, $\alpha_{2,1}$, $\phi_{2,1}$) are necessary to obtain an accurate response or not. The importance of these terms are assessed by investigating the perturbation solution when these are set to zero one at a time, as shown in Fig. 7. The response becomes inaccurate when any one of them is set to zero; all nonlinear terms are necessary to obtain an accurate response.

4.2.2 Experimental Results. In this section, experimental measurements of rotational vibration of unity ratio gear pairs with profile and lead modifications [5] are compared with the second
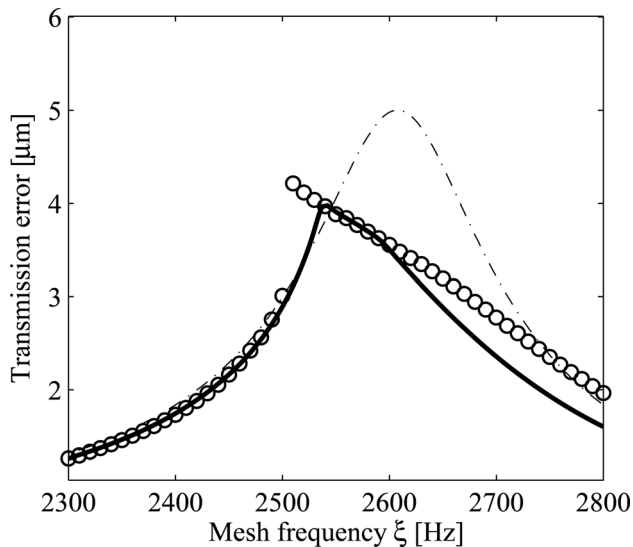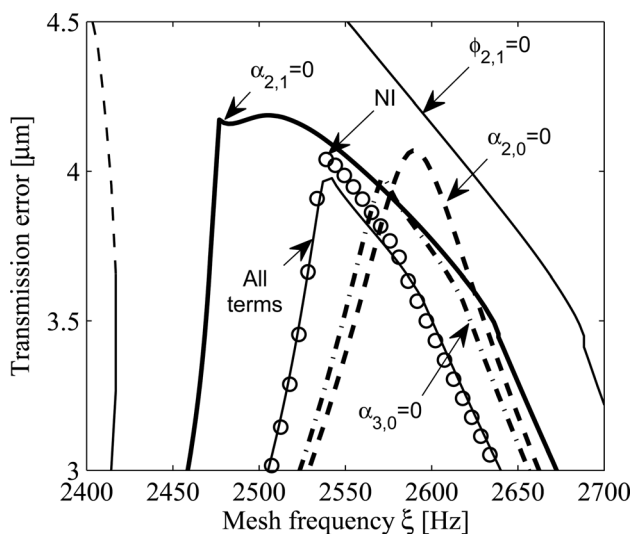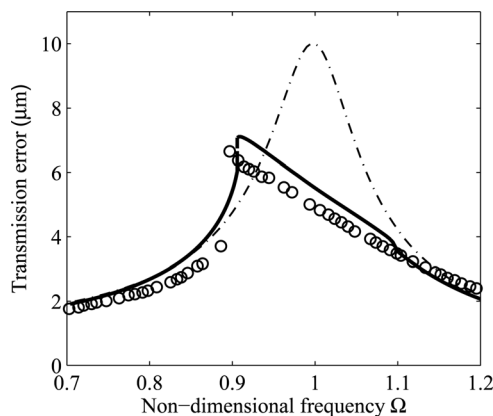
Fig. 6 Primary resonance of a helical gear pair at 200 Nm using second order perturbation, numerical integration, and the linearized model. The numerical integration results are obtained using the method of Ref. [9] (stable perturbation solution: solid line, computational data by numerical integration: circles, linear solution: dashed-dotted line).

Fig. 7 Perturbation solution when $\alpha_{2,0}$, $\alpha_{3,0}$, $\alpha_{2,1}$, and $\phi_{2,1}$ are set to zero one at a time are shown. The nonzero parameters are the same as in Fig. 6. The circles denote numerical integration with no nonzero parameters.

Table 4 Physical parameters of the spur gears analyzed in Figs. 9, 10, and 11

Parameter	Pinion	Common	Gear
Number of teeth	50		50
Transverse module (mm)	3		3
Base helix angle (deg)		0	
Transverse operating pressure angle (deg)		20.00	
Facewidth (μm)	20.00		20.00
Center distance (μm)		150.00	
Tip relief (μm)	Varies		Varies
Lead crown (μm)	5		5

Fig. 8 Force-deflection function $f(x,t)$ obtained by finite element analysis of a spur gear pair with increasing applied torque. Gear data from Ref. [5], linear tip relief of 10μm starts at 20.9 deg.

Fig. 9 Primary resonance of a spur gear pair (tip relief start at 20.9 deg) at 85 Nm using second order perturbation and linearized model. Experimental data are from Fig. 3(c) of Ref. [5] (stable second order perturbation: solid line, unstable second order perturbation solution: dashed line, experimental measurement: circles, linear solution: dashed-dotted line).
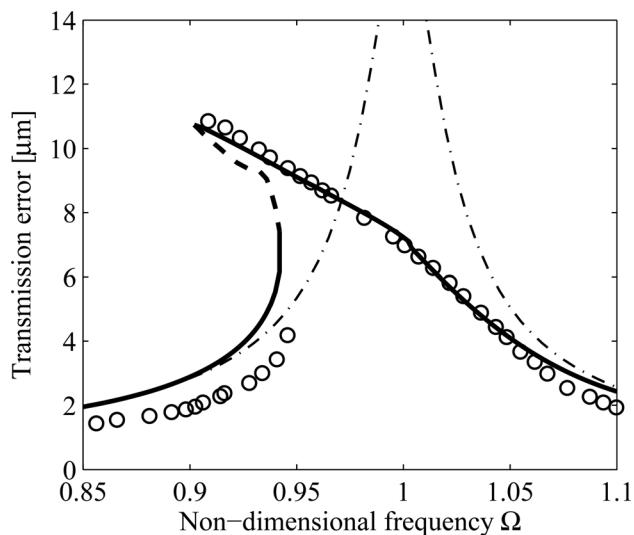
order perturbation solution. The experimental measurements are available for various tip relief starting roll angles and for different applied torques.

The gear parameters from Ref. [5] are listed in Table 4. The nondimensional parameters are given in Table 3. The gears in this test rig are sufficiently isolated from the vibrations of the supporting structure to justify use of a single degree-of-freedom oscillator to model the dynamics [24].

The force-deflection function would ideally come from the experimental setup by slowly rotating the gears through a mesh period and measuring transmission error at various applied torques. Because these data are not given, the force-deflection function is obtained from finite element analysis [43] of the gears. When the tip relief starts at roll angle 20.9 deg, the force-deflection function calculated by finite element analysis is shown in Fig. 8 for various torques. Even if the finite element analysis could precisely replicate the elastic behavior of the experimental setup, the crucial gear tooth profile and lead modifications are specified within a manufacturing tolerance (3 μm). These errors can cause a mismatch between the experimental data and perturbation solution.

Fig. 10 Primary resonance of a spur gear pair (tip relief start at 20.9 deg) at 170 Nm using second order perturbation and linearized model. Experimental data are from Fig. 3(*b*) of Ref. [5] (stable second order perturbation: solid line, unstable second order perturbation solution: dashed line, experimental measurement: circles, linear solution: dashed-dotted line).
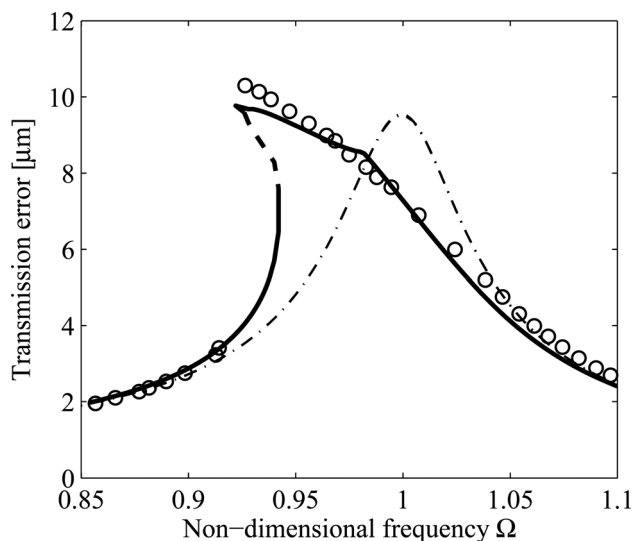
Fig. 11 Primary resonance of a spur gear pair (tip relief start at 23.6 deg) at 170 Nm using second order perturbation and linearized model. Experimental data are from Fig. 3(*b*) of Ref. [5] (stable perturbation solution: solid line, unstable perturbation solution: dashed line, experimental measurement: circles, linear solution: dashed-dotted line).

The experimental measurements and the second order perturbation solution for three gear pairs are compared in Fig. 9 (where the applied torque is 85 Nm and the 10 μm profile modification starts at 20.9 deg), Fig. 10 (where the applied torque is 170 Nm and the 10 μm profile modification starts at 20.9 deg), and Fig. 11 (where the applied torque is 170 Nm and the profile 10 μm modification starts at 23.6 deg). Table 3 lists the nondimensional parameters used in this analysis. All gears have 5 μm lead crown modification.

The perturbation solutions agree accurately with the experimental results in all three cases. Damping is estimated to be between 2% and 5% as shown in Table 3. This agrees with the reported damping of 2% in Ref. [5] and yields perturbation results that

closely match the experiments, as shown in the figures. The agreement with the experimental measurements justifies the use of the single-degree-of-freedom rotational oscillator model and the exclusion of friction forces for gear vibrations. These justifications, however, are specific to the experimental setup because compliant bearings or poorly lubricated gears with high friction may require different physical assumptions.

The onset of total contact loss is manifest by the kinks in the perturbation solution curves. Even in regions without total contact loss, the linear response differs from the experimental measurements and perturbation solutions. Region 2 of Fig. 4 characterizes this type of response. The difference is attributed to partial contact loss and occurs due to the profile and lead modifications. The good agreement provides experimental evidence that the perturbation solution predicts the nonlinear dynamic response due to partial contact loss.

5 Conclusions

This work derives approximate, closed-form analytical solutions for the nonlinear vibration of gear pairs with profile and lead modifications described by a specified nonlinear, periodic force-deflection curve. The solution includes reductions in profile and face contact ratios as a result of vibration combined with modifications. Misalignments in the gear assembly are considered by their effects on the force-deflection curve. The solution includes nonlinear effects of partial contact loss, that is, reductions in profile and face contact ratios as a result of vibration combined with tooth modifications. The method of multiple scales provides the analytical perturbation solutions in the primary resonance region.

(1) The dynamic excitation in gear pairs is mathematically shown to come from the periodicity of the force-deflection function. This periodicity is due to the periodic engagement/disengagement of the gear teeth resulting in linear and quadratic mesh stiffness fluctuations that drive the gear vibration. The occurrence of total contact loss in unmodified gears is shown to be independent of applied torque because the vibration amplitude increases with larger torques, so does the threshold of vibrations needed to trigger total contact loss. This is not true for modified gears; the occurrence of contact loss depends on applied torque in modified gears. Once contact loss starts to occur, however, the amplitude of nonlinear vibration does depend on applied torque.

(2) The method of multiple scales gives the approximate, closed-form analytical solutions, which provide physical insight on the effect of design parameters on nonlinear vibration. Comparisons with gear vibration experiments and numerical integration verify the analytical solution by perturbation. It is observed that the second order perturbation solution is significantly more accurate than the first order perturbation solution, indicating the nonlinearity is strong in the physical experiments.

(3) Key regions in the nonlinear response are:
  (a) Linear region: vibration amplitude is relatively low, and the system behaves linearly.
  (b) Partial contact loss region: The mean stiffness drops due to partial contact loss from reduced profile and face contact ratios as a result of vibration; nevertheless, contact is maintained. During partial contact loss, nominal contact lines lose contact although the gear teeth remain engaged. Partial contact loss is most prominent in systems with tooth profile and lead modifications. Quadratic and cubic nonlinearities capture the partial contact loss nonlinearity in modified gears; quadratic and cubic nonlinearities drive the nonlinear response.
  (c) Onset of total contact loss region: Vibrations reach the threshold to cause total contact loss. The onset frequency and amplitude is independent of applied torque

in unmodified gears. The amplitude and the frequency at the onset of total contact loss is analytically given and is consistent with experiments.

(d) Total contact loss region: The contact separates fully and the mean load brings the system back into contact. Total contact loss in gears occurs when the gear teeth disengage completely. When contact loss occurs, vibration amplitude depends on applied torque. Contact loss is captured by the mean reduction in mesh stiffness and its two harmonics. For contact loss, the perturbation solution considers one separation per period, and excludes further period doubling and chaos. The validity of this assumption is borne out by the correlation with experimentally measured vibration.

References

[1] Chang, S., Houser, D. R., and Harianto, J., 2003, "Tooth Flank Corrections of Wide Face Width Helical Gears That Account for Shaft Deflections," Proceedings of the ASME International Design Engineering Technical Conferences and Computers and Information in Engineering, Chicago, IL, September 2–6, ASME Paper No. DETC2003/PTG-48072.

[2] Litvin, F. L., Fuentes, A., Gonzalez-Perez, I., Carnevali, L., and Kawasaki, K., 2003, "Modified Involute Helical Gears: Computerized Design, Simulation of Meshing, and Stress Analysis," Tech. Report No. ARL-CR-514.

[3] Umezawa, K., Sato, T., and Ishikawa, J., 1984, "Simulation of Rotational Vibration of Spur Gears," Bull. JSME, **27**(223), pp. 102–109.

[4] Velex, P., and Maatar, M., 1996, "A Mathematical Model for Analyzing the Influence of Shape Deviations and Mounting Errors on Gear Dynamic Behavior," J. Sound Vib., **191**(5), pp. 629–660.

[5] Kahraman, A., and Blankenship, G. W., 1999, "Effect of Involute Tip Relief on Dynamic Response of Spur Gear Pairs," J. Mech. Des., **121**(5), pp. 313–315.

[6] Parker, R. G., Vijayakar, S. M., and Imajo, T., 2000, "Non-Linear Dynamic Response of a Spur Gear Pair: Modelling and Experimental Comparisons," J. Sound Vib., **237**(3), pp. 435–455.

[7] Ambarisha, V. K., and Parker, R. G., 2007, "Nonlinear Dynamics of Planetary Gears Using Analytical and Finite Element Models," J. Sound Vib., **302**(3), pp. 577–595.

[8] Eritenel, T., and Parker, R. G., 2011, "Nonlinear Vibration of Gear Pairs With Tooth Surface Modifications at Primary Resonance Using a Perturbation Method," Proceedings of the ASME International Design Engineering Technical Conferences and Computers and Information in Engineering, Washington, DC, August 28–31, ASME Paper No. DETC2011/MSNDC-48689.

[9] Eritenel, T., and Parker, R. G., 2012, "Three-Dimensional Nonlinear Vibration of Gear Pairs," J. Sound Vib., **331**, pp. 3628–3648.

[10] Eritenel, T., and Parker, R. G., 2012, "An Investigation of Tooth Mesh Nonlinearity and Partial Contact Loss in Gear Pairs Using a Lumped-Parameter Model," Mech. Mach. Theory, **56**, pp. 28–51.

[11] Gregory, R. W., Harris, S. L., and Munro, R. G., 1963, "Dynamic Behavior of Spur Gears," Proc. Inst. Mech. Eng., **178**(8), pp. 261–266.

[12] Andersson, A., and Vedmar, L., 2003, "A Dynamic Model to Determine Vibrations in Involute Helical Gears," J. Sound Vib., **260**(2), pp. 195–212.

[13] Baud, S., and Velex, P., 2002, "Static and Dynamic Tooth Loading in Spur and Helical Geared Systems-Experiments and Code Validation," ASME J. Mech. Des., **124**(2), pp. 334–346.

[14] Kubur, M., Kahraman, A., Zini, D. M., and Kienzle, K., 2004, "Dynamic Analysis of a Multi-Shaft Helical Gear Transmission by Finite Elements: Model and Experiment," ASME J. Vib. Acoust., **126**(3), pp. 398–406.

[15] Ajmi, M., and Velex, P., 2005, "A Model for Simulating the Quasi-Static and Dynamic Behaviour of Solid Wide-Faced Spur and Helical Gears," Mech. Mach. Theory, **40**(2), pp. 173–190.

[16] Harris, S. L., 1958, "Dynamic Loads on the Teeth of Spur Gears," IMechE Appl. Mech., **172**, pp. 87–100.

[17] Singh, R., Houser, D. R., and Kahraman, A., 1990, "Non-Linear Dynamic Analysis of Geared Systems," Tech. Report No. NASA-CR-180495.

[18] Özgüven, H. N., and Houser, D. R., 1988, "Mathematical-Models Used in Gear Dynamics—A Review," J. Sound Vib., **121**(3), pp. 383–411.

[19] Özgüven, H. N., and Houser, D. R., 1988, "Dynamic Analysis of High Speed Gears by Using Loaded Static Transmission Error," J. Sound Vib., **125**(1), pp. 71–83.

[20] Lee, C., Lin, H.-H., Oswald, F. B., and Townsend, D. P., 1991, "Influence of Linear Profile Modification and Loading Conditions on the Dynamic Tooth Load and Stress of High-Contact-Ratio Spur Gears," ASME J. Mech. Des., **113**(4), pp. 473–480.

[21] Velex, P., and Ajmi, M., 2006, "On the Modelling of Excitations in Geared Systems by Transmission Errors," J. Sound Vib., **290**(3–5), pp. 882–909.

[22] Liu, G., and Parker, R. G., 2008, "Dynamic Modeling and Analysis of Tooth Profile Modification for Multimesh Gear Vibration," ASME J. Mech. Des., **130**(2), p. 121402.

[23] Kahraman, A., and Singh, R., 1990, "Non-Linear Dynamics of a Spur Gear Pair," J. Sound Vib., **142**(1), pp. 49–75.

[24] Blankenship, G. W., and Kahraman, A., 1995, "Steady State Force Response of a Mechanical Oscillator With Combined Parametric Excitation and Clearance Type Non-Linearity," J. Sound Vib., **185**(5), pp. 743–765.

[25] Padmanabhan, C., and Singh, R., 1996, "Analysis of Periodically Forced Nonlinear Hill's Oscillator With Application to a Geared System," J. Acoust. Soc. Am., **99**(1), pp. 324–334.

[26] Kahraman, A., and Blankenship, G. W., 1996, "Interactions Between Commensurate Parametric and Forcing Excitations in a System With Clearance," J. Sound Vib., **194**(3), pp. 317–336.

[27] Kahraman, A., and Singh, R., 1991, "Interactions Between Time-Varying Mesh Stiffness and Clearance Non-Linearities in a Geared System," J. Sound Vib., **146**(1), pp. 135–156.

[28] Theodossiades, S., and Natsiavas, S., 2000, "Non-Linear Dynamics of Gear-Pair Systems With Periodic Stiffness and Backlash," J. Sound Vib., **229**(2), pp. 287–310.

[29] Natsiavas, S., Theodossiades, S., and Goudas, I., 2000, "Dynamic Analysis of Piecewise Linear Oscillators With Time Periodic Coefficients," Int. J. Nonlinear Mech., **35**(1), pp. 53–68.

[30] Liu, G., and Parker, R. G., 2008, "Nonlinear Dynamics of Idler Gear Systems," Nonlinear Dyn., **53**(4), pp. 345–367.

[31] Kubo, A., 1978, "Stress Condition, Vibration Exciting Force and Contact Pattern of Helical Gears With Manufacturing and Alignment Error," ASME J. Mech. Des., **100**, pp. 77–84.

[32] Matsumura, S., Umezawa, K., and Houjoh, H., 1996, "Rotational Vibration of a Helical Gear Pair Having Tooth Surface Deviation During Transmission of Light Load," JSME Int. J., Ser. C, **39**(3), pp. 614–620.

[33] Velex, P., Maatar, M., and Raclot, J. P., 1997, "Some Numerical Methods for the Simulation of Geared Transmission Dynamic Behavior Formulation and Assessment," ASME J. Mech. Des., **119**(2), pp. 292–298.

[34] Raclot, J. P., and Velex, P., 1999, "Simulation of the Dynamic Behaviour of Single and Multi-Stage Geared Systems With Shape Deviations and Mounting Errors by Using a Spectral Method," J. Sound Vib., **220**(5), pp. 861–903.

[35] Kubo, A., Kiyono, S., and Makoto, F., 1986, "On Analysis and Prediction of Machine Vibration Caused by Gear Meshing: 1st Report, Nature of Gear Vibration and the Total Vibrational Excitation," Bull. JSME, **29**(258), pp. 4424–4429.

[36] Kahraman, A., and Blankenship, G. W., 1999, "Effect of Involute Contact Ratio on Spur Gear Dynamics," ASME J. Mech. Des., **121**(1), pp. 112–118.

[37] Bahk, C.-J., and Parker, R. G., 2011, "Analytical Solution for the Nonlinear Dynamics of Planetary Gears," J. Comput. Nonlinear Dyn., **6**(2), p. 021007.

[38] Blankenship, G. W., and Kahraman, A., 1996, "Gear Dynamics Experiments Part 1: Characterization of Forced Response," Proceedings of the ASME Design Engineering Technical Conferences, Irvine, CA, August 18–22.

[39] Nayfeh, A. H., and Mook, D. T., 1979, *Nonlinear Oscillations*, Wiley, New York.

[40] Nayfeh, A. H., 1993, *Problems in Perturbation*, John Wiley & Sons, New York.

[41] Zhu, F., and Parker, R. G., 2006, "Perturbation Analysis of a Clearance-Type Nonlinear System," J. Sound Vib., **292**(3–5), pp. 969–979.

[42] Luongo, A., and Paolone, A., 1999, "On the Reconstitution Problem in the Multiple Time-Scale Method," Nonlinear Dyn., **19**(2), pp. 133–156.

[43] Vijayakar, S. M., 1991, "A Combined Surface Integral and Finite-Element Solution for a Three-Dimensional Contact Problem," Int. J. Numer. Methods Eng., **31**(3), pp. 525–545.